

# Theoretical Insights into the Retinal Dynamics of Vascular Endothelial Growth Factor in Patients Treated with Ranibizumab, Based on an Ocular Pharmacokinetic/Pharmacodynamic Model

Laurence A. Hutton-Smith,<sup>\*,†</sup> Eamonn A. Gaffney,<sup>†</sup> Helen M. Byrne,<sup>†</sup> Antonello Caruso,<sup>‡,ib</sup> Philip K. Maini,<sup>†</sup> and Norman A. Mazer<sup>\*,‡,ib</sup>

<sup>†</sup>Wolfson Centre for Mathematical Biology, Mathematical Institute, Andrew Wiles Building, University of Oxford, Radcliffe Observatory Quarter, Woodstock Road, Oxford OX2 6GG, U.K.

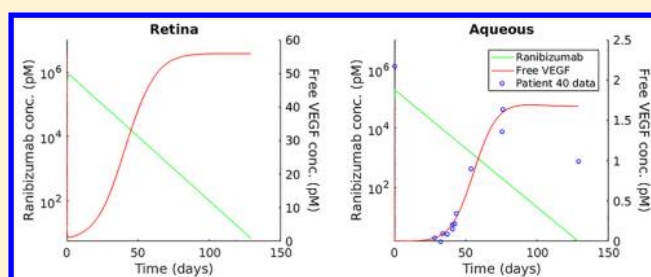
<sup>‡</sup>Roche Pharma Research and Early Development, Pharmaceutical Sciences, Roche Innovation Center Basel, F. Hoffmann-La Roche Ltd, Grenzacherstrasse 124, 4070 Basel, Switzerland

## Supporting Information

**ABSTRACT:** Neovascular age-related macular degeneration (wet AMD) results from the pathological angiogenesis of choroidal capillaries, which leak fluid within or below the macular region of the retina. The current standard of care for treating wet AMD utilizes intravitreal injections of anti-VEGF antibodies or antibody fragments to suppress ocular vascular endothelial growth factor (VEGF) levels. While VEGF suppression has been demonstrated in wet AMD patients by serial measurements of free-VEGF concentrations in aqueous humor samples, it is presumed that anti-VEGF molecules also

permeate across the inner limiting membrane (ILM) of the retina as well as the retinal pigmented epithelium (RPE) and suppress VEGF levels in the retina and/or choroidal regions. The latter effects are inferred from serial optical coherence tomography (OCT) measurements of fluid in the retinal and sub-retinal spaces. In order to gain theoretical insights to the dynamics of retinal levels of free-VEGF following intravitreal injection of anti-VEGF molecules, we have extended our previous two-compartment pharmacokinetic/pharmacodynamic (PK/PD) model of ranibizumab–VEGF suppression in vitreous and aqueous humors to a three-compartment model that includes the retinal compartment. In the new model, reference values for the macromolecular permeability coefficients between retina and vitreous ( $p_{ILM}$ ) and between retina and choroid ( $p_{RPE}$ ) were estimated from PK data obtained in rabbit. With these values, the three-compartment model was used to re-analyze the aqueous humor levels of free-VEGF obtained in wet AMD patients treated with ranibizumab and to compare them to the simulated retinal levels of free-VEGF, including the observed variability in PK and PD. We have also used the model to explore the impact of varying  $p_{ILM}$  and  $p_{RPE}$  to assess the case in which an anti-VEGF molecule is impermeable to the ILM and to assess the potential effects of AMD pathology on the RPE barrier. Our simulations show that, for the reference values of  $p_{ILM}$  and  $p_{RPE}$ , the simulated duration of VEGF suppression in the retina is approximately 50% shorter than the observed duration of VEGF suppression in the aqueous humor, a finding that may explain the short duration of suppressed disease activity in the “high anti-VEGF demand” patients reported by Fauser and Muether (*Br. J. Ophthalmol.* **2016**, *100*, 1494–1498). At 10-fold lower values of  $p_{RPE}$ , the durations of VEGF suppression in the retina and aqueous humor are comparable. Lastly we have used the model to explore the impact of dose and binding parameters on the duration and depth of VEGF suppression in the aqueous and retinal compartments. Our simulations with the three-compartment PK/PD model provide new insights into inter-patient variability in response to anti-VEGF therapy and offer a mechanistic framework for developing treatment regimens and molecules that may prolong the duration of retinal VEGF suppression.

**KEYWORDS:** retina, intravitreal, ranibizumab pharmacokinetics, VEGF pharmacodynamics, permeability, mechanistic modeling, neovascular age-related macular degeneration



## INTRODUCTION

Neovascular age-related macular degeneration (wet AMD), a debilitating retinal disease causing central vision loss and blindness, predominately affecting the elderly population, is predicted to afflict 200 million people globally by 2020.<sup>1</sup> Symptoms of wet AMD are theorized to occur due to the proliferation of poorly formed and highly permeable capillaries

through the posterior of the retina, causing the buildup of fluid within the macula, disrupting photoreceptor cell structure and

Received: March 15, 2018

Revised: May 3, 2018

Accepted: May 7, 2018

Published: May 7, 2018

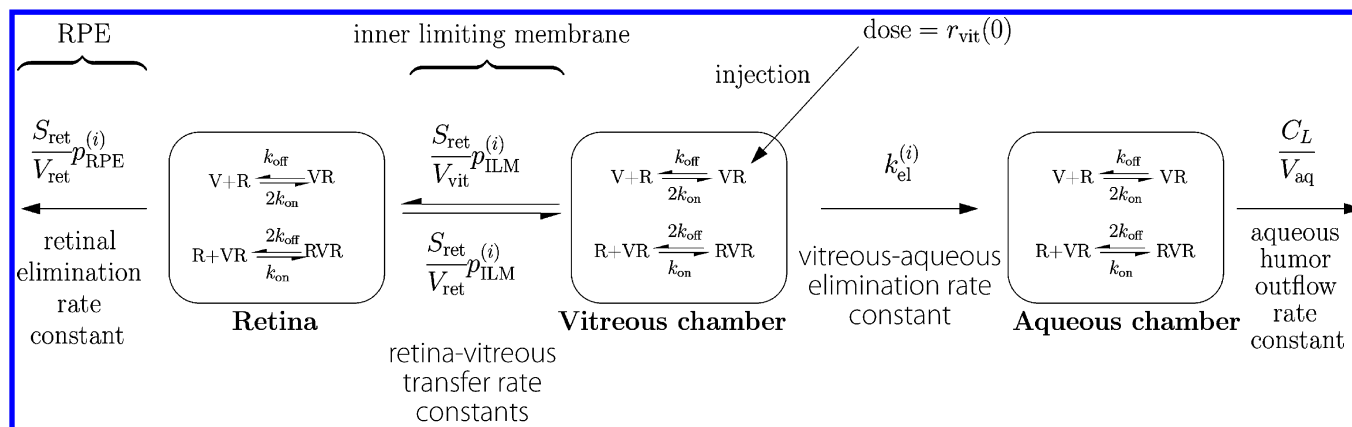


**Figure 1.** Three-compartment reaction model diagram. Transport pathways, with their respective transfer rate constants, are indicated by arrows between compartments. Reactions between chemical species, e.g., R, V, VR, and RVR, are shown with their respective reaction rates inside compartments, where  $S_{ret}$ ,  $V_{ret}$ ,  $V_{vit}$ ,  $V_{aq}$ ,  $p_{RPE}^{(i)}$ ,  $p_{ILM}^{(i)}$ ,  $k_{el}^{(i)}$ , and  $C_L$  represent the retinal surface area, retinal volume (including both the intracellular and extracellular spaces), vitreal volume, aqueous volume, RPE permeability, ILM permeability, vitreous–aqueous elimination rate, and clearance from the aqueous chamber, respectively. The superscript ( $i$ ) denotes parameters whose values depend on the hydrodynamic radius of the particular chemical species  $i$ .  $r_{vit}(t)$  represents the vitreal concentration of unbound ranibizumab, and  $r_{ret}(0)$  represents the initial drug concentration.

degrading visual acuity.<sup>2</sup> This angiogenic process is thought to be initiated and perpetuated by the production of vascular endothelial growth factor (VEGF) within the eye.<sup>3,4</sup> Current treatments for wet AMD utilize anti-VEGF macromolecules, given by intravitreal (IVT) injection. Such molecules bind to VEGF, blocking its interaction with endothelial cells on the surface of neovascular capillaries, attempting to inhibit further angiogenesis and fluid leakage.<sup>5</sup>

It is generally assumed that, to achieve maximum angiogenic inhibition, anti-VEGF molecules must bind to VEGF molecules within and below the retina. To do this, after IVT injection, molecules must diffuse to and penetrate through the inner limiting membrane (ILM) to enter the retina, and then subsequently through the retinal pigment epithelium (RPE) to enter sub-retinal space. Assessing drug and/or VEGF binding in these tissue layers would require serial retinal biopsies and is not therefore feasible in wet AMD patients. On the other hand, serial aqueous humor samples can be obtained from wet AMD patients and have been used by Fauser and colleagues to characterize the VEGF suppression time (VST) associated with different anti-VEGF compounds.<sup>6,7</sup> While there appears to be a general association between the aqueous humor VST and the suppression of clinical disease activity assessed by optical coherence tomography (OCT) or visual acuity on a population basis, it is presently unknown if the pharmacodynamics (PD) of VEGF suppression in the retina is similar to the PD observed in aqueous humor and/or whether it would more closely parallel the disease activity in individual patients. The recent observation that the aqueous humor VST is approximately twice as long as the period of suppressed disease activity in a specific subgroup of patients with “persistent [choroidal neovascularization] activity during anti-VEGF treatment”<sup>7</sup> suggests that the retinal VST could be shorter than the aqueous VST, at least in some patients.

To address these questions, we present a three-compartment (retina, vitreous, and aqueous) ocular pharmacokinetic/pharmacodynamic (PK/PD) model, developed by combining a previously presented three-compartment PK model<sup>8</sup> and a two-compartment (vitreous and aqueous) PK/PD model.<sup>9</sup> To predict retinal PD, we used the three-compartment PK/PD model to re-analyze a clinical data set<sup>10</sup> containing free VEGF

aqueous humor samples taken from patients with wet-AMD undergoing treatment with ranibizumab (an anti-VEGF antibody fragment<sup>11</sup>).

The extension from a two- to three-compartment PK/PD model grants the ability to compare the simulated free (unbound) VEGF concentration profiles of the retina, vitreous, and aqueous compartments. We therefore present an analysis of the temporal behavior between these three compartments, as well as an analysis of the changes in retinal and aqueous PD induced through the alteration of dose and binding kinetics. Our analysis shows that, under certain conditions, a temporal disparity may exist between the suppression of free VEGF levels in the retina and aqueous humor, as well as a difference in the suppression magnitude. Alongside these results, we also present two case studies addressing relevant biological scenarios, simulation of which was not possible with previous ocular models.

## METHODS

**Experimental and Clinical Data.** The three-compartment PK/PD developed here is built upon a three-compartment PK model presented by Hutton-Smith et al. in 2017,<sup>8</sup> with the addition of ranibizumab–VEGF binding kinetics. Specifically this paper utilizes relationships derived from experimental PK data in the rabbit,<sup>12</sup> between the retinal permeability coefficients ( $p_{ILM}$  and  $p_{RPE}$ ) and hydrodynamic radius given by Hutton-Smith et al.<sup>8</sup>

For the analysis presented in this study, we utilized the 2015 data set published by Saunders<sup>10</sup> and previously analyzed by Hutton-Smith et al.,<sup>9</sup> detailing 31 patients with neovascular age-related macular degeneration (wet AMD). Aqueous humor samples were collected at several time points post intravitreal (IVT) injection of 0.5 mg of ranibizumab, as well as a pre-treatment baseline sample. Free VEGF concentration was then determined for each sample using Luminex multiplex bead analysis (Luminex, Austin, TX, USA). Data presented in the supporting file from ref 10 were originally digitized using Plot Digitizer Version 2.0 (Department of Physics, University of South Alabama) in ref 9.

**Model Description.** The three-compartment PK/PD model, described graphically in Figure 1, is comprised of the

retina, vitreous humor, and aqueous humor, between which transport pathways are shown, denoted by arrows, alongside their corresponding transfer rate constant expressions. Reaction kinetics between chemical species can occur within any of the three model compartments: VEGF ( $V$ ) has two identical binding sites to which ranibizumab ( $R$ ) can bind<sup>3</sup> to form a VEGF–ranibizumab complex ( $VR$ ) and subsequently a ranibizumab–VEGF–ranibizumab complex ( $RVR$ ). Reactions are governed by eqs 1 and 2, in which  $k_{\text{on}}$  and  $k_{\text{off}}$  (and hence also the dissociation constant  $K_D = k_{\text{off}}/k_{\text{on}}$ ) are reaction rates corresponding to a hypothetical single VEGF binding site.



Chemical species concentrations in each compartment, with units of pM, are denoted by  $v(t)$ ,  $r(t)$ ,  $c(t)$ , and  $h(t)$  for  $V$ ,  $R$ ,  $VR$ , and  $RVR$ , respectively. Subscripts on chemical concentrations denote the compartment to which they refer; for example,  $r_{\text{vit}}(t)$  describes the concentration of  $R$  in the vitreous. Full details on concentration notation can be found in Table 1.

Table 1. Model Chemical Species<sup>a</sup>

species	conc (in pM)	description
$V_{\text{ret}}$	$v_{\text{ret}}$	VEGF
$R_{\text{ret}}$	$r_{\text{ret}}$	ranibizumab
$VR_{\text{ret}}$	$c_{\text{ret}}$	VEGF–ranibizumab complex
$RVR_{\text{ret}}$	$h_{\text{ret}}$	ranibizumab–VEGF–ranibizumab complex
$V_{\text{vit}}$	$v_{\text{vit}}$	VEGF
$R_{\text{vit}}$	$r_{\text{vit}}$	ranibizumab
$VR_{\text{vit}}$	$c_{\text{vit}}$	VEGF–ranibizumab complex
$RVR_{\text{vit}}$	$h_{\text{vit}}$	ranibizumab–VEGF–ranibizumab complex
$V_{\text{aq}}$	$v_{\text{aq}}$	VEGF
$R_{\text{aq}}$	$r_{\text{aq}}$	ranibizumab
$VR_{\text{aq}}$	$c_{\text{aq}}$	VEGF–ranibizumab complex
$RVR_{\text{aq}}$	$h_{\text{aq}}$	ranibizumab–VEGF–ranibizumab complex

<sup>a</sup>All concentrations are functions of time ( $t$ ), and subscripts indicate the compartment associated with each concentration.

Throughout this publication, we will refer to VEGF that is not bound in a  $VR$  or  $RVR$  complex as “free VEGF”, whereas we refer to unbound ranibizumab simply as “ranibizumab”, as typically the concentration of unbound ranibizumab is several orders of magnitude greater than that of  $VR$  or  $RVR$ . Initially, prior to IVT injection, VEGF levels are assumed to be at their respective steady-state levels in all compartments, and all complexes are assumed to have zero concentration. Ranibizumab is taken to have zero retinal and aqueous concentration initially, and a vitreal concentration  $r_{\text{vit}}(0)$  corresponding to a dose of 0.5 mg, calculated using the molecular weight of ranibizumab, taken to be 48.35 kDa.<sup>11</sup>

The model schematic in Figure 1 is then formulated, using parameters listed in Table 2, into the following nonlinear system of ordinary differential equations (where  $k_{\text{on}} = k_{\text{off}}/K_D$ ):

•Retina

Table 2. Model Parameters<sup>a</sup>

parameter	value	units	description
$k_{\text{off}}$	0.864 (ref 14)	day <sup>-1</sup>	single binding site off rate
$K_D$	estimated	pM	single binding site model dissociation constant
$V_{\text{in}}$	disease state dep.	fmol/day	rate of VEGF production
$t_{1/2}^{(i)}$	$R_i$ dep.	days	ocular half-life <sup>c</sup>
$k_{\text{el}}^{(i)}$	$R_i$ dep.	day <sup>-1</sup>	vitreous–aqueous elimination rate constant
$p_{\text{RPE}}^{(i)}$	eq 15	cm/s	RPE permeability
$p_{\text{ILM}}^{(i)}$	eq 16	cm/s	ILM permeability
$C_L$	3.6 (ref 15)	mL/day	clearance from the aqueous chamber
$v_{\text{ret}}$	0.22 <sup>b</sup>	mL	retinal volume
$V_{\text{vit}}$	4.5 (refs 16, 17)	mL	vitreous volume
$V_{\text{aq}}$	0.16 (refs 18, 19)	mL	aqueous volume
$S_{\text{ret}}$	9.71 <sup>b</sup>	cm <sup>2</sup>	retinal surface area

<sup>a</sup>Entries with superscript ( $i$ ) are chemical species specific, where  $i$  corresponds to  $V$ ,  $R$ ,  $VR$ , or  $RVR$ . <sup>b</sup>These values were calculated by taking the cross-sectional retinal distance from the posterior to the anterior as 2.37 cm (estimated from Missel<sup>20</sup>), the retinal thickness as 0.022 cm,<sup>20</sup> and retinal radius equivalent to that of a sphere of volume 4.5 mL, in the same manner as presented by Hutton-Smith et al.<sup>8</sup> <sup>c</sup>This is the apparent half-life, which describes the rate of decay in all three compartments, as motivated by ref 8.

$$\frac{dv_{\text{ret}}}{dt} = (k_{\text{off}}c_{\text{ret}} - 2k_{\text{on}}v_{\text{ret}}r_{\text{ret}}) - \frac{S_{\text{ret}}}{V_{\text{ret}}}(p_{\text{ILM}}^{(v)} + p_{\text{RPE}}^{(v)})v_{\text{ret}} + \frac{S_{\text{ret}}}{V_{\text{ret}}}p_{\text{ILM}}^{(v)}v_{\text{vit}} + \frac{V_{\text{in}}}{V_{\text{ret}}} \quad (3)$$

$$\frac{dr_{\text{ret}}}{dt} = (k_{\text{off}}c_{\text{ret}} - 2k_{\text{on}}v_{\text{ret}}r_{\text{ret}}) + (2k_{\text{off}}h_{\text{ret}} - k_{\text{on}}r_{\text{ret}}c_{\text{ret}}) - \frac{S_{\text{ret}}}{V_{\text{ret}}}(p_{\text{ILM}}^{(r)} + p_{\text{RPE}}^{(r)})r_{\text{ret}} + \frac{S_{\text{ret}}}{V_{\text{ret}}}p_{\text{ILM}}^{(r)}r_{\text{vit}} \quad (4)$$

$$\frac{dc_{\text{ret}}}{dt} = -(k_{\text{off}}c_{\text{ret}} - 2k_{\text{on}}v_{\text{ret}}r_{\text{ret}}) + (2k_{\text{off}}h_{\text{ret}} - k_{\text{on}}r_{\text{ret}}c_{\text{ret}}) - \frac{S_{\text{ret}}}{V_{\text{ret}}}(p_{\text{ILM}}^{(c)} + p_{\text{RPE}}^{(c)})c_{\text{ret}} + \frac{S_{\text{ret}}}{V_{\text{ret}}}p_{\text{ILM}}^{(c)}c_{\text{vit}} \quad (5)$$

$$\frac{dh_{\text{ret}}}{dt} = -(2k_{\text{off}}h_{\text{ret}} - k_{\text{on}}r_{\text{ret}}c_{\text{ret}}) - \frac{S_{\text{ret}}}{V_{\text{ret}}}(p_{\text{ILM}}^{(h)} + p_{\text{RPE}}^{(h)})h_{\text{ret}} + \frac{S_{\text{ret}}}{V_{\text{ret}}}p_{\text{ILM}}^{(h)}h_{\text{vit}} \quad (6)$$

•Vitreous

$$\frac{dv_{\text{vit}}}{dt} = (k_{\text{off}}c_{\text{vit}} - 2k_{\text{on}}v_{\text{vit}}r_{\text{vit}}) + \frac{S_{\text{ret}}}{V_{\text{vit}}}p_{\text{ILM}}^{(v)}v_{\text{ret}} - \frac{S_{\text{ret}}}{V_{\text{vit}}}p_{\text{ILM}}^{(v)}v_{\text{vit}} - k_{\text{el}}^{(v)}v_{\text{vit}} \quad (7)$$

$$\frac{dr_{\text{vit}}}{dt} = (k_{\text{off}}c_{\text{vit}} - 2k_{\text{on}}v_{\text{vit}}r_{\text{vit}}) + (2k_{\text{off}}h_{\text{vit}} - k_{\text{on}}r_{\text{vit}}c_{\text{vit}}) + \frac{S_{\text{ret}}}{V_{\text{vit}}}p_{\text{ILM}}^{(r)}r_{\text{ret}} - \frac{S_{\text{ret}}}{r_{\text{vit}}}p_{\text{ILM}}^{(r)}r_{\text{vit}} - k_{\text{el}}^{(r)}r_{\text{vit}} \quad (8)$$

$$\frac{dc_{vit}}{dt} = -(k_{off}c_{vit} - 2k_{on}v_{vit}r_{vit}) + (2k_{off}h_{vit} - k_{on}r_{vit}c_{vit}) + \frac{S_{ret}}{V_{vit}}p_{ILM}^{(c)}c_{ret} - \frac{S_{ret}}{c_{vit}}p_{ILM}^{(c)}c_{vit} - k_{el}^{(c)}c_{vit} \quad (9)$$

$$\frac{dh_{vit}}{dt} = -(2k_{off}h_{vit} - k_{on}r_{vit}c_{vit}) + \frac{S_{ret}}{V_{vit}}p_{ILM}^{(h)}h_{ret} - \frac{S_{ret}}{h_{vit}}p_{ILM}^{(h)}h_{vit} - k_{el}^{(h)}h_{vit} \quad (10)$$

•Aqueous

$$\frac{dv_{aq}}{dt} = (k_{off}c_{aq} - 2k_{on}v_{aq}r_{aq}) + \frac{V_{vit}}{V_{aq}}k_{el}^{(v)}v_{vit} - \frac{C_L}{V_{aq}}v_{aq} \quad (11)$$

$$\frac{dr_{aq}}{dt} = (k_{off}c_{aq} - 2k_{on}v_{aq}r_{aq}) + (2k_{off}h_{aq} - k_{on}r_{aq}c_{aq}) + \frac{V_{vit}}{V_{aq}}k_{el}^{(r)}r_{vit} - \frac{C_L}{V_{aq}}r_{aq} \quad (12)$$

$$\frac{dc_{aq}}{dt} = -(k_{off}c_{aq} - 2k_{on}v_{aq}r_{aq}) + (2k_{off}h_{aq} - k_{on}r_{aq}c_{aq}) + \frac{V_{vit}}{V_{aq}}k_{el}^{(c)}c_{vit} - \frac{C_L}{V_{aq}}c_{aq} \quad (13)$$

$$\frac{dh_{aq}}{dt} = -(2k_{off}h_{aq} - k_{on}r_{aq}c_{aq}) + \frac{V_{vit}}{V_{aq}}k_{el}^{(h)}h_{vit} - \frac{C_L}{V_{aq}}h_{aq} \quad (14)$$

Transport rate constants between compartments, as noted earlier, are shown in Figure 1 next to their respective pathways. Transport is permitted between the vitreous chamber and the retina in either direction, with rate described via the permeability,  $p_{ILM}$  (cm/s), of the inner limiting membrane (ILM), a basement membrane structure<sup>13</sup> found between the retina and vitreous chamber. Unidirectional transport from the vitreous to the aqueous is also permitted and regulated by the transport rate constant  $k_{el}$  (1/day). Clearance occurs in the retina, through the retinal pigment epithelium (RPE), with rate described in terms of the permeability,  $p_{RPE}$  (cm/s), of the RPE, as well as in the aqueous chamber,  $C_L$  (mL/day), assumed to equal the rate of aqueous humor production.

All transport rates, excluding the elimination rate from the aqueous humor, are functions of the hydrodynamic radius,  $R_h$  (nm), and differ for all chemical species (whose values of  $R_h$  can be found in Table 3). Superscripts on transport rates and permeabilities indicate this chemical species dependence; for

**Table 3. Hydrodynamic Radii and Retinal Permeabilities for Molecular Species<sup>a</sup>**

chemical species	notation	hydrodynamic radius (nm)	$p_{RPE}^{(i)}$ ( $\times 10^{-7}$ cm/s)	$p_{ILM}^{(i)}$ ( $\times 10^{-7}$ cm/s)
V	$R_h^{(v)}$	2.39	2.66	1.89
R	$R_h^{(r)}$	2.45	2.63	1.89
VR	$R_h^{(v)}$	3.29	2.28	1.79
RVR	$R_h^{(h)}$	4.07	2.06	1.73

<sup>a</sup>Values were calculated by modeling each species as a prolate ellipsoid, the method for which is described in Section S1 of the Supporting Information.

example,  $p_{RPE}^{(v)}$  would be the permeability of the RPE to VEGF. The equations determining the hydrodynamic radius dependence for retinal permeabilities are taken from Hutton-Smith et al.,<sup>8</sup> who estimated power law expressions for these parameters using *in vivo* rabbit PK data for antibody and antibody fragments collected by Gadkar et al.<sup>12</sup> The expression, in terms of hydrodynamic radius, for  $p_{RPE}$  is given by

$$p_{RPE}^{(i)}(R_h) = 4.04 \times 10^{-7} R_h^{-0.48} \quad (15)$$

and  $p_{ILM}$  is found via the following expression:

$$p_{ILM}^{(i)}(R_h) = 2.2 \times 10^{-7} R_h^{-0.17} \quad (16)$$

where both  $p_{RPE}^{(i)}$  and  $p_{ILM}^{(i)}$  have units of cm/s, and  $R_h$  has units of nm. We have investigated the consequences of scaling  $p_{RPE}^{(i)}(R_h)$  by factors of 10 and 0.1 in order to illustrate the sensitivity of the model to the magnitude of  $p_{RPE}$ , which could conceivably be modified by the penetration of neovascular blood vessels through the RPE and/or the presence of drusen beneath the RPE. We have also investigated the case of a drug that is unable to permeate across the ILM to see how the binding of VEGF in the vitreous influences the retinal concentration of VEGF.

To calculate the molecule-specific elimination rate constant  $k_{el}^{(i)}$ , we note that Hutton-Smith et al.<sup>9</sup> demonstrated that the  $t_{1/2}$  of a molecule can be considered proportional to its hydrodynamic radius. Therefore, by fixing a value for the half-life of ranibizumab,  $t_{1/2}^{(r)}$ , we may estimate  $t_{1/2}(R_h)$  for other chemical species via the following formula:

$$t_{1/2}(R_h) = \left( \frac{t_{1/2}^{(r)}}{R_h^{(r)}} \right) R_h \quad (17)$$

With a known half-life, the long time decay rate  $\lambda$  for a molecule of hydrodynamic radius  $R_h$  can then be described by

$$\lambda(R_h) = \frac{\log 2}{t_{1/2}(R_h)} \quad (18)$$

The vitreous–aqueous rate constant  $k_{el}^{(i)}$  (shown in Figure 1) can be estimated from  $\lambda^{(i)}$ ,  $p_{ILM}^{(i)}$ ,  $p_{RPE}^{(i)}$ , and the anatomical factors  $V_{vit}$ ,  $S_{ret}$ , and  $v_{ret}$  as shown in Section S2 of the Supporting Information. The model is then formulated, in terms of the parameters in Table 2, into a nonlinear system of 12 ordinary differential equations, with initial conditions found in Section S3 of the Supporting Information, representing equilibrium VEGF levels and an initial IVT dose of ranibizumab. Parameters for scaled permeability case studies are generated by completing the steps described above and then scaling  $p_{RPE}^{(i)}$  post hoc; in this way  $k_{el}^{(i)}$  remains unchanged but  $t_{1/2}^{(i)}$  is changed. To investigate the effect of modifying dosage and reaction rates, we altered the parameters  $r_{vit}(0)$ ,  $K_D$ ,  $k_{off}$ , and  $k_{on}$ , given a fixed half-life and VEGF production rate.

**Fitting Protocol.** Equations 3–14 were solved numerically in MATLAB using `ode23s` and fit to each of the 31 patient data sets using `lsqnonlin`<sup>21</sup> (part of MATLAB's global optimization toolbox). A range of fixed  $K_D$  values (between 50 and 50 000 pM) were analyzed; during the fitting protocol, a value of  $K_D$  within this range was taken and kept fixed, while  $t_{1/2}^{(r)}$  and  $V_{in}$  were varied by the fitting algorithm, penalizing the relative mean square error between the logarithms of the numerical solution and the data. This process was repeated for every patient over the given range of  $K_D$  values, yielding a

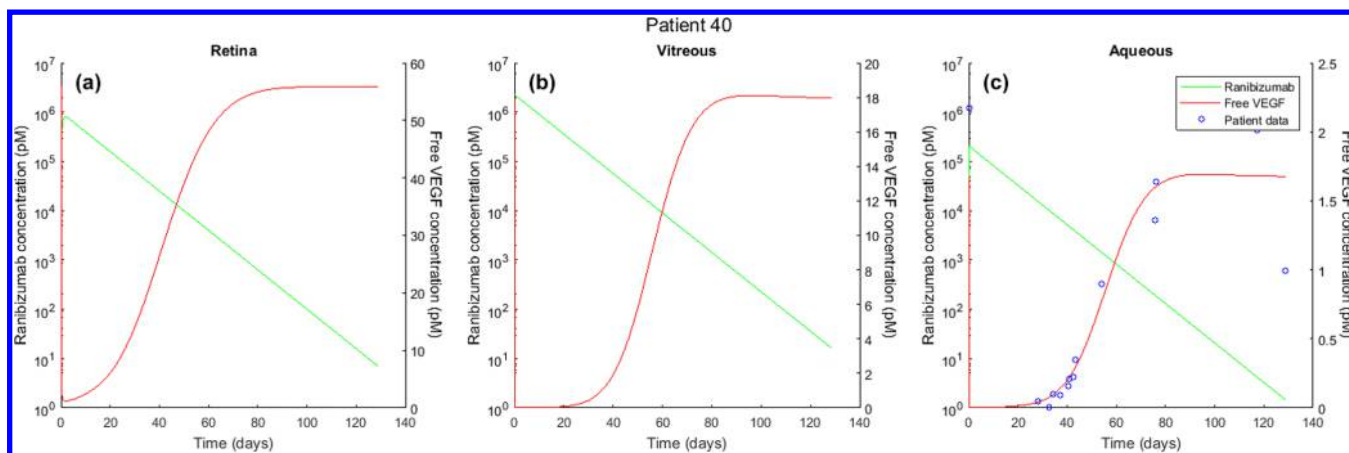


**Figure 2.** Fitting result for patient 40. Concentration profiles of free VEGF and ranibizumab in the retina (a), vitreous (b), and aqueous (c), plotted with optimal parameters, with values  $K_D = 19\,000$  pM,  $V_{in} = 18.5$  fmol/day, and  $t_{1/2}^{(r)} = 7.5$  days. Patient data can be seen in the aqueous in blue; in all three compartments, ranibizumab (log scale, left axis) and VEGF (linear scale, right axis) concentrations are shown in green and red, respectively.

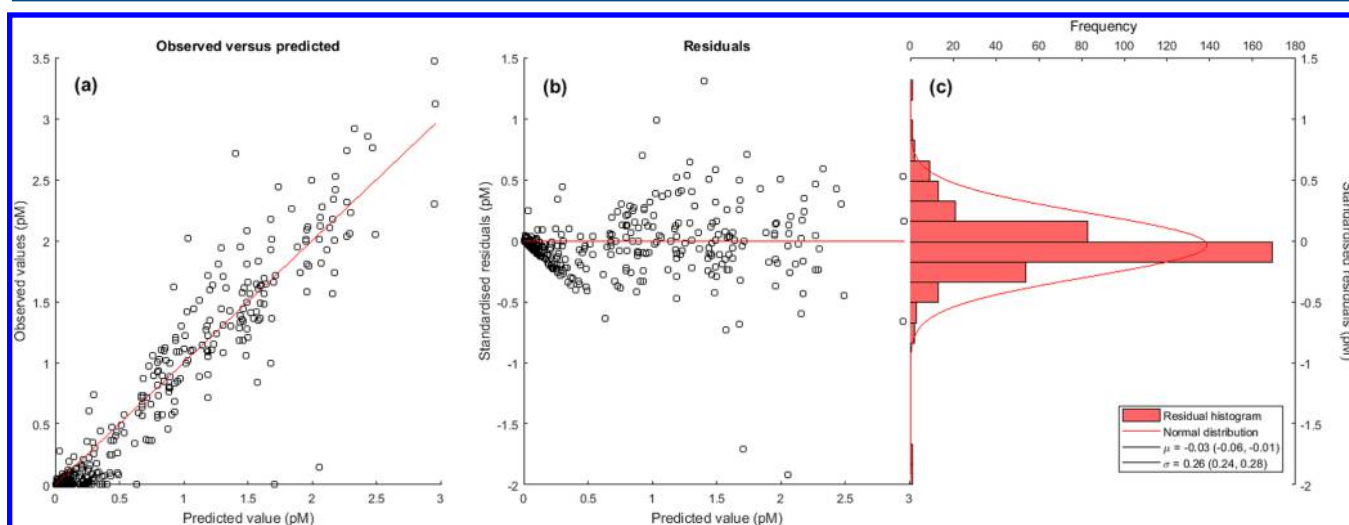


**Figure 3.** Comparison between observed data points across all 31 patients, and the corresponding predictions made by the model. (a) The two quantities plotted versus each other, with the red line representing perfect correlation. (b) Difference for each data point between the predicted and observed values, alongside (c) a plot of their distribution and inferred normal distribution.

distribution of predicted values for  $t_{1/2}^{(r)}$  and  $V_{in}$  over the patient sample for each analyzed value of  $K_D$ . Through this method (identical to that presented in ref 9), the resultant values of  $t_{1/2}^{(r)}$  were compared to experimental data ( $7.9 (\pm 1.74)$  days, previously compiled in ref 9) in order to estimate the value of  $K_D$ . The distribution of predicted  $t_{1/2}^{(r)}$  and  $V_{in}$  values was fit to a log-normal distribution using the `lognfit`<sup>21</sup> function of MATLAB.

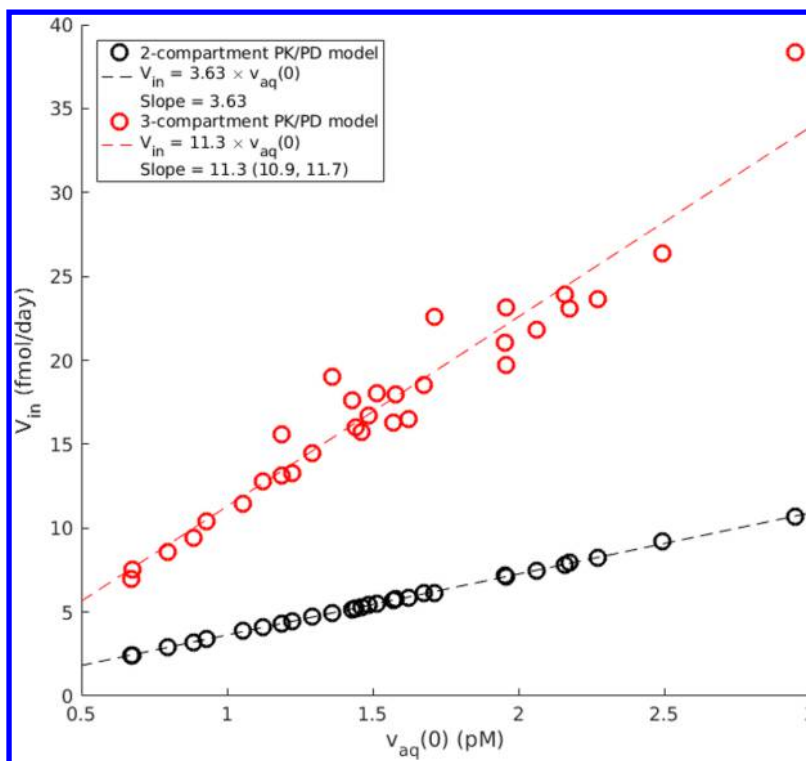
## RESULTS

**Fitting Results.** The model was found to fit well to the data set from Saunders et al.<sup>10</sup> A representative patient's fit (patient 40) can be seen in Figure 2, with full results from the fitting protocol provided in Section S4 of the Supporting Information, where individual patient fits and parameters are given. The *in vivo* dissociation constant between VEGF and ranibizumab,  $K_D$ , was estimated to have a value 19 000 pM. In Figure 2 we see the simulated time dependence of ranibizumab and the free VEGF concentrations in the retina, vitreous, and aqueous compartments and the corresponding data VEGF data in the aqueous compartment. Ranibizumab decays exponentially at

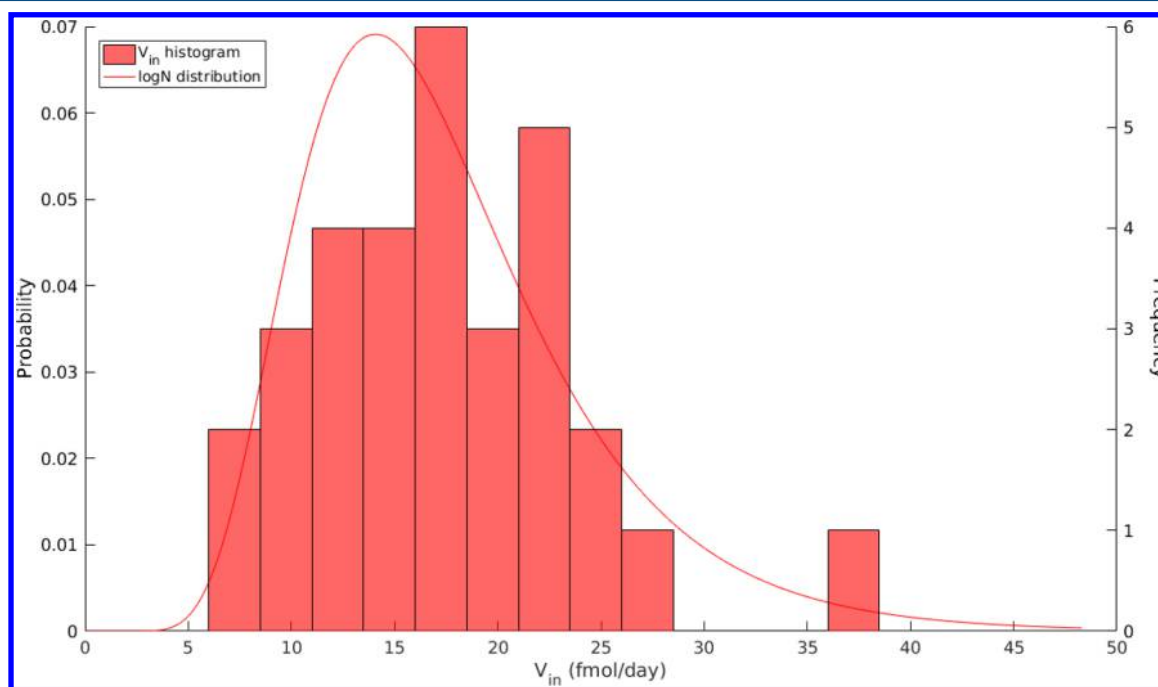
the same rate in all three compartments of the model, and the vitreous concentration is approximately 10× greater than that of the aqueous, and approximately 2× greater than that of the retina. The free VEGF concentrations in vitreous and aqueous chambers return to their initial values in parallel; however, the retina returns to steady state before both the vitreous and aqueous. We also note that the initial value of free VEGF in the retina is approximately 3× greater than that of the vitreous, and approximately 30× greater than that of the aqueous.

Figure 3a compares the observed and predicted VEGF data points in the aqueous humor from all patients and observation times, demonstrating that the model performs well across the patient data set. Figure 3b,c shows that the residuals appear to be normally distributed with mean and standard deviation of approximately 0 and 0.26 pM, respectively.

**VEGF Production Rate.** Figure 4 shows the estimates of  $V_{in}$  for the present three-compartment model and the prior two-compartment model vs the steady-state aqueous humor VEGF concentration for each subject. The slope for the three-compartment model is approximately 3-fold larger than for the two-compartment model. Section S3 of the Supporting



**Figure 4.** Predicted VEGF production rates,  $V_{in}$  (fmol/day), over the patient sample for  $K_D = 19\,000$  pM.  $V_{in}$  is plotted for each patient versus their aqueous free VEGF steady-state concentration level,  $v_{aq}(0)$  (pM). Red dots are  $V_{in}$  levels predicted by the modeling work performed in this study; black dots are the predicted  $V_{in}$  values, derived from the same data set, by the two-compartment model presented in ref 9.



**Figure 5.** Distribution of  $V_{in}$  over patient sample for  $K_D = 19\,000$  pM. A fit log-normal distribution is shown by the red line, with parameters (95% CI)  $\mu = 2.76$  (2.65, 2.93) and  $\sigma = 0.38$  (0.30, 0.51).

**Information** shows that the slope for the two-compartment model is identical to  $C_D$ , while the slope for the three-compartment model depends on additional parameters. This difference in VEGF production implies that approximately 70% of VEGF is eliminated via the choroid relative to 30% eliminated via the aqueous.

**Figure 5** shows the distribution of predicted  $V_{in}$  values across the patient sample. Modeling these data with a log-normal distribution,<sup>22</sup> we find they have mean and standard deviation of 17.5 and 6.9 fmol/day, respectively. As shown in **Figure 4**, the variation in these predicted values is a direct consequence

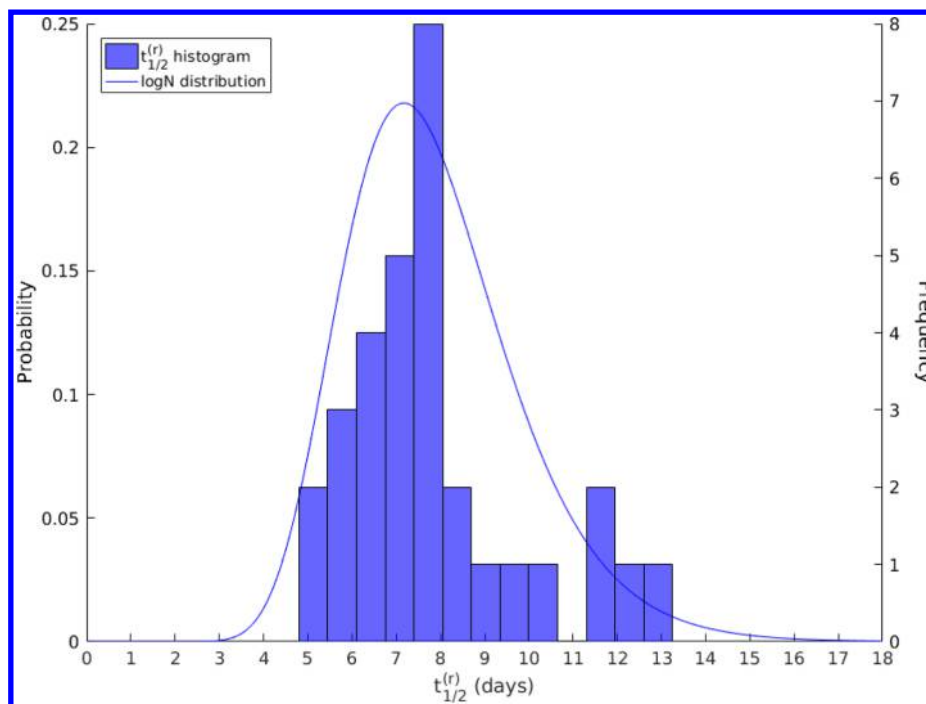


**Figure 6.** Distribution of  $t_{1/2}^{(r)}$  over patient sample for  $K_D = 19\,000$  pM. The box plot is a histogram, whereas the line shows a log-normal distribution, fit to these data, with parameters (95% CI)  $\mu = 2.03$  (1.94, 2.12) and  $\sigma = 0.25$  (0.20, 0.33).

of the variation in observed aqueous equilibrium free VEGF concentration and demonstrates inter-patient variability.

#### Inter-patient Variation in $t_{1/2}^{(r)}$ and Free VEGF Profiles.

In addition to the VEGF production rate, there is large variation across the patient sample over the time course of the free VEGF profiles. This is quantified by the fitting process (for a fixed value of  $K_D$ ) through variation in the ocular half-life of ranibizumab  $t_{1/2}^{(r)}$  and related species. The distribution of predicted values of  $t_{1/2}^{(r)}$  is shown in Figure 6, also modeled as a log-normal distribution.<sup>22</sup> The predicted log-normal parameters (as shown in the figure legend) predict a mean  $t_{1/2}^{(r)}$  of 7.9 days, with a standard deviation of 2.0 days.

By normalizing the free VEGF profile for each patient, the temporal variation found within the patient sample can be visualized. The shaded regions shown in Figure 7 correspond to the range of simulated free VEGF profiles (which can be seen plotted for each individual in Section S4 of the Supporting Information); the red and blue regions represent the retina and aqueous, respectively. Panel (a) of Figure 7 superimposes the normalized clinical data; one can see the consistency between the distribution of the model fits and the data points. Note the difference between panels (a) (aqueous) and (b) (retina) within the first 30 days. Here we see a distinct difference in behavior: the aqueous profiles all drop to zero within  $0 < t \ll 1$  day, whereas the retina reaches a non-zero minimum in roughly 2 days, at which point it starts growing exponentially.

We note that in Figure 7 data points that lie outside of the shaded 10–90th percentile region may be in either the 0–10th or 90–100th half-life percentile. Additionally, other points may lay outside due to variability in determining the baseline VEGF production rate.

**Retina–Aqueous Suppression Lag.** As noted previously, the retina begins returning to its free VEGF steady-state concentration sooner than the vitreous and aqueous (which return in parallel at a later time). We define  $t_{\text{ret}}^{(10\%)}$  and  $t_{\text{aq}}^{(10\%)}$  as the times for the retina and aqueous to return to 10% of their

respective compartment VEGF steady-state concentration. Figure 8 shows  $t_{\text{ret}}^{(10\%)}$  plotted versus  $t_{\text{aq}}^{(10\%)}$  for all 31 patients, demonstrating a strong linear correlation, indicating that the retina reaches 10% of its respective free VEGF concentration approximately twice as fast as the aqueous. We also note that average value of  $t_{\text{ret}}^{(10\%)}$  is approximately 20 days shorter than the average value of  $t_{\text{aq}}^{(10\%)}$ , across the patient sample.

**Simulated Pharmacodynamics for a Drug Impermeable to the Retina.** Currently it is assumed that an IVT drug for wet AMD is required to permeate through the ILM and into the retina to be efficacious;<sup>23</sup> however, it is not known whether a drug that cannot penetrate into the retina can still lower retinal VEGF levels by vitreal binding alone. This scenario can be simulated using our model by setting the ILM permeability to drug and drug–VEGF complexes to zero. The numerical solution for retinal free VEGF, of a simulated IVT of 0.5 mg dose of retina-impermeable drug, can be seen in Figure 9. The drop in VEGF concentration is only roughly 15% of the steady-state VEGF concentration, after which the concentration of free VEGF returns to steady state. The concentration to which VEGF initially falls is equal to

$$v_{\text{ret}}(t) \simeq \frac{V_{\text{in}}}{S_{\text{ret}}(p_{\text{ILM}}^{(v)} + p_{\text{RPE}}^{(v)})}, \quad 0 < t \ll 50 \text{ days} \quad (19)$$

This expression does not contain any drug-related parameters; therefore, the model predicts that if a drug is unable to permeate from the vitreous to the retina, then the concentration to which free VEGF falls in the retina is independent of any properties of the drug, providing it is sufficiently mobile to justify the use of the well-mixed approximation implemented here. The expression given by eq 19 is simply the steady-state solution for  $v_{\text{ret}}$  derived from eq 3, by setting  $v_{\text{vit}} = 0$  in the absence of drug in the retina ( $c_{\text{ret}} = r_{\text{ret}} = 0$ ). This scenario is equivalent to that in which all VEGF in the vitreous is initially assumed to be bound.

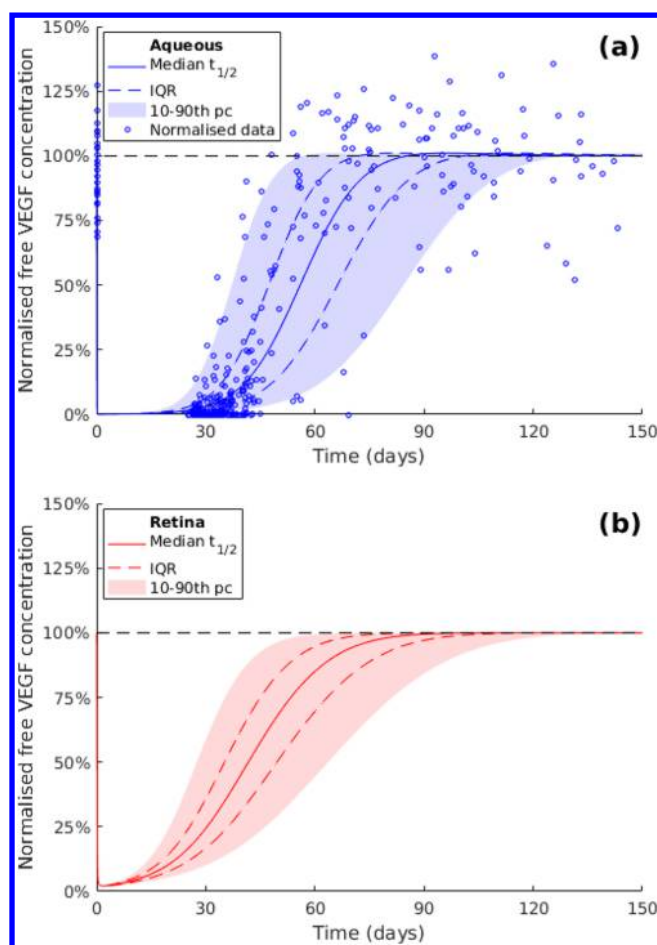


**Figure 7.** Range of normalized free VEGF concentrations across patient sample. The shaded red and blue regions represent the aqueous (a) and retina (b). Panel (a) also shows the normalized clinical data. Patient simulations shown are fits corresponding to  $K_D = 19\,000$  pM.

### Impact of Alterations to the Permeability of the RPE.

Here we consider the possibility that pRPE may be affected by disease processes that either increase permeability, e.g., penetration of choroidal neovascularization through the RPE, or decrease permeability, e.g., large drusen in the Bruch's membrane.

In Figure 10 we see the simulated effect of varying  $p_{RPE}$  by factors of 10 and 0.1, relative to the nominal values estimated in the rabbit model, for two distinct dosage regimens, 0.5 and 2 mg. When  $p_{RPE}$  is increased, we see a sharp leftward shift in the retinal free VEGF profile, reduced retinal area under the curve of ranibizumab, and decreased  $t_{1/2}$  equal to 6.6 days. Relative to the solid red curve, the dashed red curve indicates little free VEGF suppression. Conversely, when  $p_{RPE}$  is decreased, we see increased free VEGF suppression in the both the retina and aqueous, as well as an increased  $t_{1/2}$ , equal to 9.6 days. Note that retinal concentrations are more strongly affected by the value of  $p_{RPE}$  than the aqueous concentrations. The blue lines in Figure 10 demonstrate the effect of increasing the dose from 0.5 to 2 mg. In panels (e) and (f) we see that the blue lines are vertical translations of the corresponding red lines, as would be expected for an increase in dosage. In panels (c) and (d) we see that the effect of increasing the dose manifests as a rightward shift in the suppression profiles, increasing the duration and magnitude of free VEGF suppression.

### Effects of Dosage and Reaction Rate Modifications.

The three-compartment model allows us, for the first time, to compare the simulated free VEGF concentration profiles of the retina and aqueous. We present an analysis examining the dynamical changes in these two compartments resulting from altering dosage and binding kinetics. The left-hand-side panels in Figures 11–14 show the free VEGF concentration in retinal compartment, alongside a magnification of the first 25 days, whereas the right-hand-side panels show analogous plots for the aqueous compartment. All simulations discussed below used  $t_{12}^{(r)} = 7.5$  days and a constant VEGF production rate of 18.5 fmol/day. The boxed regions in each plot have width of 30 days and height corresponding to 10% of their respective compartment's free VEGF steady-state concentration (this boxed region is then magnified within the panel inset); dots within the retinal inset indicate the minimum free VEGF concentration.

Figures 12–14 examine the simulated effect of varying parameters determining binding kinetics, namely  $K_D$ ,  $k_{off}$  and  $k_{on}$ , while Figure 11 shows the effect of increasing the intravitreal dose with constant binding parameters. Figure 11 demonstrates the effect of increasing the dose from the standard dose of 0.5 mg up to 4 mg. Here we see a congruent effect in both the retina and aqueous, with a rightward translation of the free VEGF profiles, equal to one half-life of ranibizumab.

In Figure 12 we see the effect of lowering  $K_D$  while keeping  $k_{on}$  constant (therefore also lowering  $k_{off}$ ). Here we see a shift of the concentration profile of the aqueous similar to that observed in Figure 11, as was also predicted by Hutton-Smith et al.,<sup>9</sup> however the model does not predict the same dynamical change in the retina. In the latter, on a longer time scale, we see a rightward temporal shift, however to a much smaller magnitude than is seen in the aqueous. At early time (<30 days) in the retina we see almost no difference.

In Figure 13 we see the effect of increasing  $k_{on}$  while keeping  $K_D$  constant (therefore also increasing  $k_{off}$ ). On a longer time scale we see very little change in either the retina or aqueous, suggesting that these compartments are in a state of chemical equilibrium. At early time in the retina we see a decrease in the maximum suppression of free VEGF, as well as a decrease in the rate of return from suppression. This follows the same dynamical change that is presented when the dosage is increased.

In Figure 14 we see the effect of increasing  $k_{on}$  while keeping  $k_{off}$  constant (therefore also lowering  $K_D$ ). We see a congruent shift to the right of free VEGF profiles between the retina and aqueous, resulting in an equal increase in  $t_{ret}^{(10\%)}$  in both compartments. In the retina, in addition to increased the suppression time, we also see a decrease in the maximum suppression of free VEGF. Here we see an almost exact reflection of the dynamical change observed upon increasing the dose: a rightward temporal shift observed in both the retina and aqueous, a decrease in the minimum achieved free VEGF retinal concentration, and a decreased rate of return from suppression.

## 5. DISCUSSION

We have shown how, through the additional estimation of retinal permeabilities, the two-compartment PK/PD model presented by Hutton-Smith et al. in 2016<sup>9</sup> may be extended to also provide a window into retinal PD. This three-compartment PK/PD model provides the first insights into the predicted behavior of free VEGF concentrations in the retina, in a way

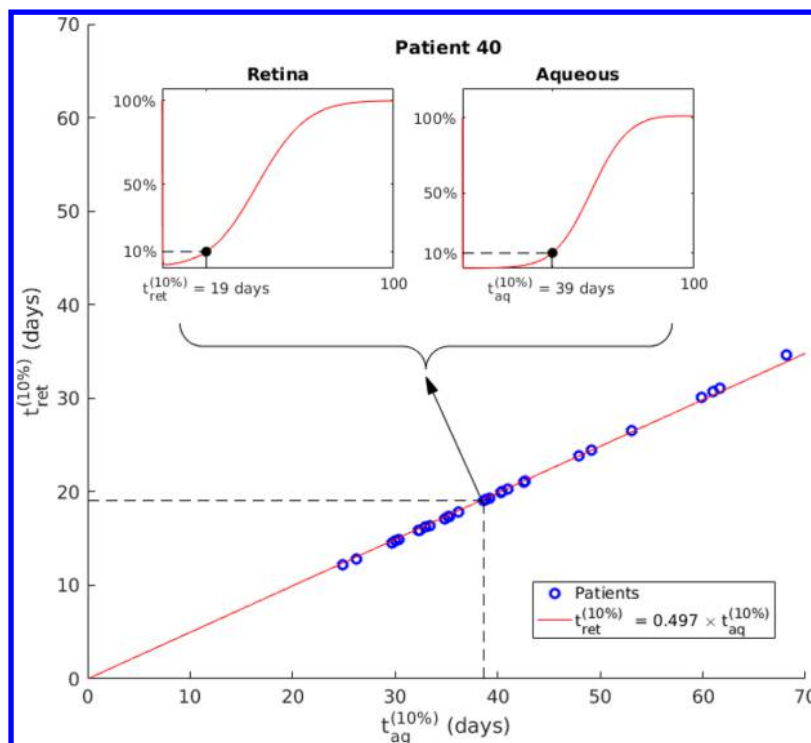


**Figure 8.** Time taken to reach 10% of VEGF steady-state concentration in the retina and aqueous, denoted by  $t_{ret}^{(10\%)}$  and  $t_{aq}^{(10\%)}$ , respectively, in days. The main plot shows patient  $t_{ret}^{(10\%)}$  values versus  $t_{aq}^{(10\%)}$ , with a linear fit through the origin, whose slope (with 95% confidence interval) is found in the legend. Using patient 40 as an example, the insets graphically describe how the terms  $t_{ret}^{(10\%)}$  and  $t_{aq}^{(10\%)}$  are defined and how the values in the main plot were generated.

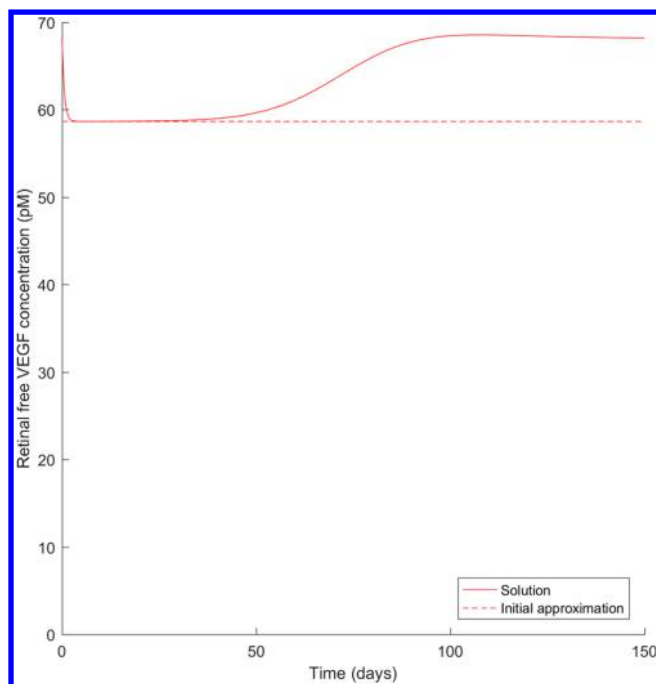


**Figure 9.** Simulated PD for a drug (and drug-VEGF complexes) impermeable to the retina. Numerical solution for an IVT dose of 0.5 mg, with  $K_D = 19\,000$  pM and half-life of 7.5 days, is shown by the solid red line. The approximation given by eq 19 is shown by the dashed line.

that cannot be directly observed clinically in humans. OCT measurements allow for the direct observation of the effect of anti-VEGF therapy on retinal disease activity; however the

relationship of OCT parameters, e.g., central retinal thickness, to retinal VEGF levels has not been established—a metric, if possible to measure clinically, would be useful in evaluating the performance of anti-VEGF molecules. The three-compartment model offers several key findings regarding an observed temporal disparity between the PD observed in the retina and aqueous humor, as well as its dependence on key parameters. This is of particular note as previous models<sup>9,10,12</sup> have assumed the behavior of free VEGF in the vitreous and aqueous to be identical to that of the retina; however, our findings suggest this is not necessarily the case.

It is important to bear in mind that the results presented in this publication are simulated predictions and are subject to the accuracy of our model assumptions. The underlying PK structure of the model was based upon the work of Hutton-Smith et al. in 2017.<sup>8</sup> A key assumption in that work was that human and rabbit retinal permeabilities are sufficiently similar; this uncertainty motivated the sensitivity study (under the heading [Impact of Alterations to the Permeability of the RPE](#) in the Results section) regarding the magnitude of  $p_{RPE}$ . Figure 10 demonstrates that, as the value of  $p_{RPE}$  is varied over 2 orders of magnitude, there is a large variation in the degree to which retinal free VEGF is suppressed, as well as in the value of  $t_{1/2}^{(r)}$ , ranging from 6.6 to 9.6 days. This variation in  $t_{1/2}^{(r)}$  due to the variation in  $p_{RPE}$  may explain, to some degree, the level of variation for a fixed value of  $K_D$ , observed in the estimated  $t_{1/2}^{(r)}$  value within the data set reported by Saunders et al.<sup>10</sup> (see Figure 6).

In Figure 9 we show the predicted retinal free VEGF profile in the case where no drug, or drug-bound VEGF molecule, is able to permeate into the retina. This result demonstrates that, if the drug is restricted from entering the retina, its ability to

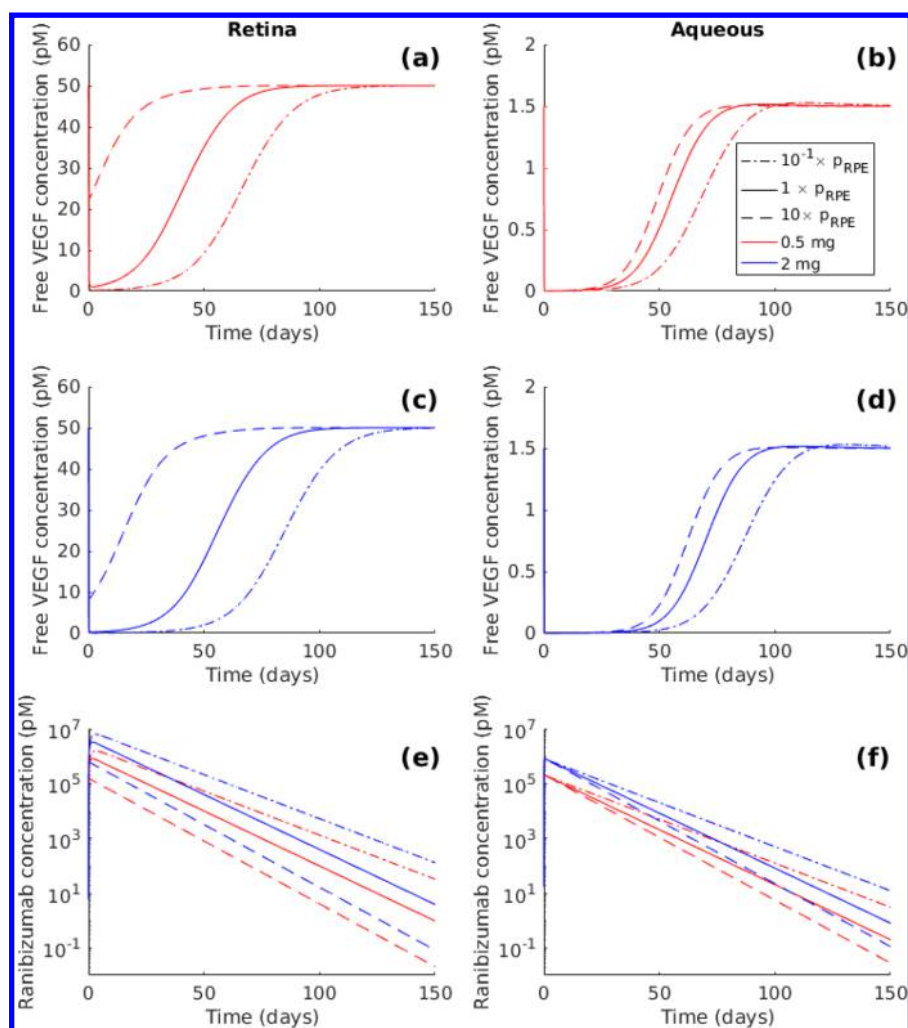


**Figure 10.** Simulated effect of varying  $p_{RPE}$  by factors of 10 and 0.1, relative to the nominal values estimated in the rabbit model, for two distinct dosage regimens: (a–d) free VEGF and (e,f) ranibizumab. Solid curves have  $p_{RPE}$  set to baseline value, as given by eq 15; dashed curves have  $p_{RPE}$  set to 10 times the solid red curve; and the dot-dashed curve has a value of  $p_{RPE}$  10 times less. Red lines represent a dose of 0.5 mg, whereas blue lines represent a dose of 2 mg. When the value of  $p_{RPE}$  is altered to the value of  $t_{1/2}^{(10)}$ , the solid, dashed, and dot-dashed curves (in the retina and aqueous humor) have  $t_{1/2}$  values of 7.5, 6.6, and 9.6 days, respectively. In these simulations  $K_D = 19\,000$  pM, and for each case  $V_{in}$  has been adjusted so as to keep the same free VEGF steady state as the base case.

suppress retinal free VEGF is largely compromised, reducing the concentration by only 15% from the steady state in Figure 9. It is known from *in vivo* and *in vitro* studies that full-length and fragment antibody molecules are able to permeate retinal membranes,<sup>12,24</sup> and given that bevacizumab is known to be an efficacious treatment for wet AMD,<sup>25</sup> we conclude that this result is not relevant to anti-VEGF macromolecules currently used in treatment. However, given that the model predicts that vitreous-to-retina penetration is necessary to maximize retinal free VEGF suppression, this may be important to consider in the development of future anti-VEGF molecules, for example, macromolecules intentionally developed to have a large hydrodynamic radius (for example, through pegylation<sup>26</sup>).

A disparity between the retina and aqueous humor is the time at which the free VEGF is predicted to return to baseline (or a percentage thereof). Figure 8 shows the time taken for the concentration of free VEGF to return to 10% of its steady-state value,  $t_{ret}^{(10\%)}$  and  $t_{aq}^{(10\%)}$ , for the retina and aqueous, respectively. From this we can see that the time taken for the concentration of retinal free VEGF to return to 10% is half of that of the aqueous. This temporal disparity, alongside the decrease in

absolute retinal free VEGF suppression relative to the aqueous, is non-optimal given that the retina is the intended site of drug action—hence, we believe investigation into the existence of this predicted phenomenon may be warranted. A study that may give credence to these predictions was conducted in a population of wet AMD patients responding poorly to anti-VEGF treatment (characterized as having a “high anti-VEGF-A demand”) by Fauser et al. in 2016.<sup>7</sup> In that work the duration of drug efficacy was demonstrated to be 14 ( $\pm 12$ ) days, as inferred using OCT measurements for a 0.5 mg dosing regimen of ranibizumab. This duration was approximately half of the VEGF suppression time measured in the aqueous humor of these patients. The return of disease activity in the retina observed by Fauser et al. appears to follow the return of retinal free VEGF that our model predicts for our base values of  $p_{RPE}$  (Figure 8). Although there is uncertainty in the levels of retinal VEGF that are needed to drive disease activity, as well as the potential for inter-patient variation in  $p_{RPE}$ , our simulations provide a plausible mechanistic hypothesis for the apparent temporal difference in retinal disease activity and aqueous

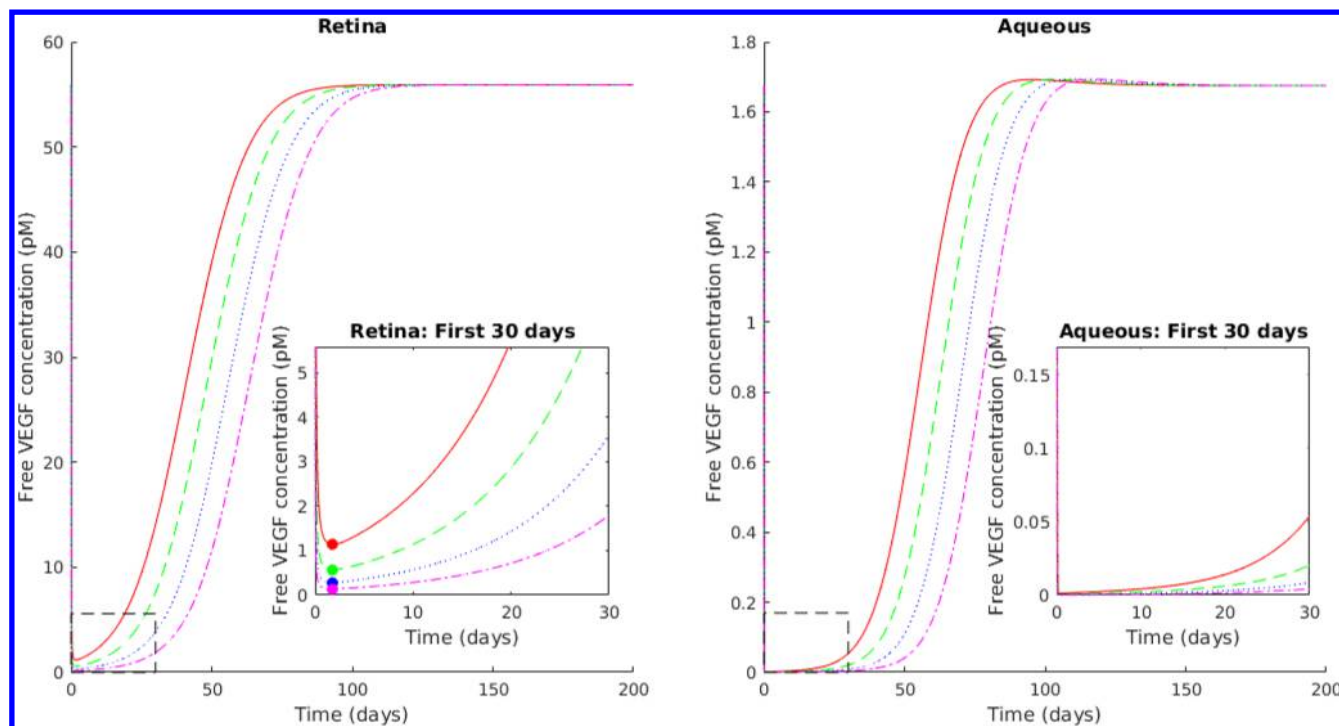


**Figure 11.** Simulated effect of increasing the dose from 0.5 mg (solid red) to 1 mg (dashed green), 2 mg (dotted blue), and 4 mg (dot-dash magenta). Plotted with  $K_D = 19\,000$  pM and  $k_{off} = 0.864$  day<sup>-1</sup>.

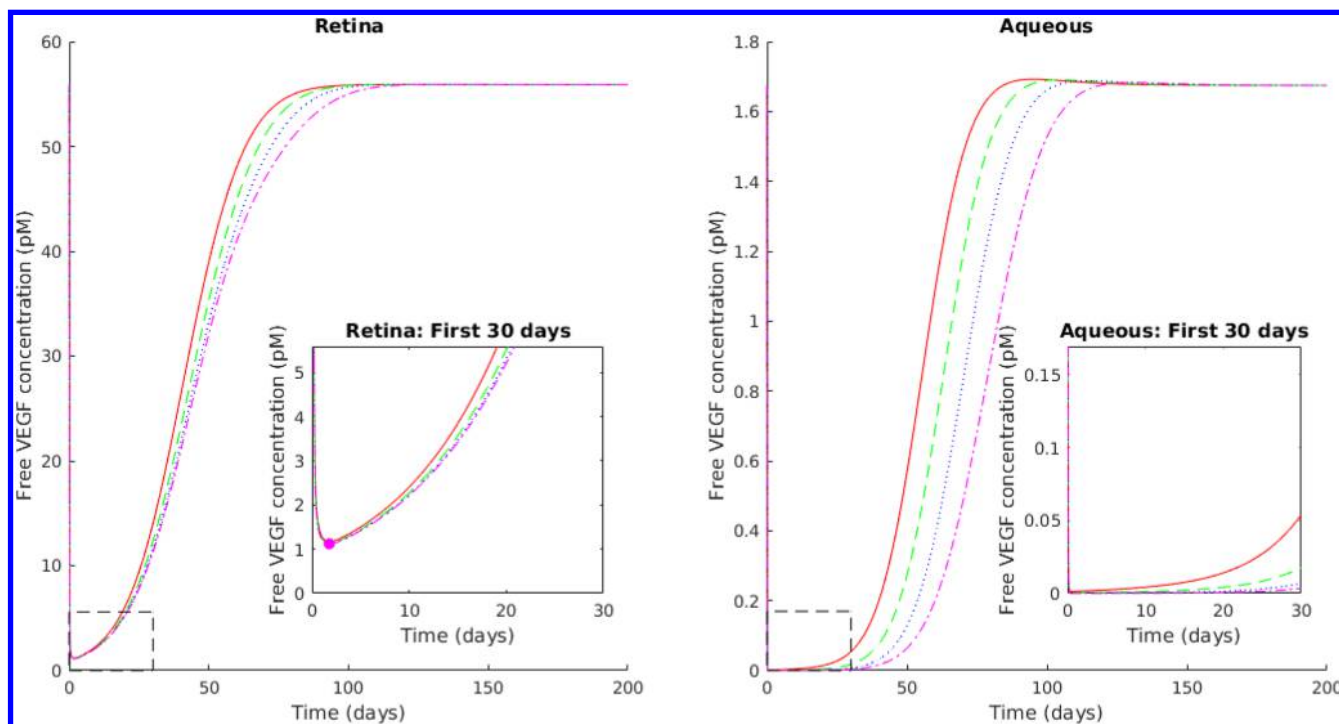


**Figure 12.** Simulated effect of decreasing  $K_D$  and  $k_{off}$  so as to keep  $k_{on}$  fixed at  $4.54$  pM<sup>-1</sup> day<sup>-1</sup>. Plots shown correspond to  $K_D = 19\,000$  pM (solid red),  $K_D = 9500$  pM (dashed green),  $K_D = 4750$  pM (dotted blue), and  $K_D = 1900$  pM (dot-dash magenta).

VEGF suppression observed in this particular sub-population of wet AMD patients.

In contrast to the subset of “high anti-VEGFA demand” patients, Fauser’s group<sup>27</sup> has previously shown that the recurrence of disease activity in the majority of wet AMD patients generally occurs after the suppression of aqueous humor VEGF levels has ended, and in some cases it may be

delayed considerably. In the present model the duration of retinal suppression of VEGF approaches the duration of aqueous humor suppression at very low values of  $p_{RPE}$  but never exceeds it (Figure 10a,b). Thus, retinal VEGF levels appear to be necessary but not sufficient to drive disease activity in some patients. The concept of what it means for free VEGF to be clinically “suppressed” is not well defined. Saunders et al.<sup>10</sup>

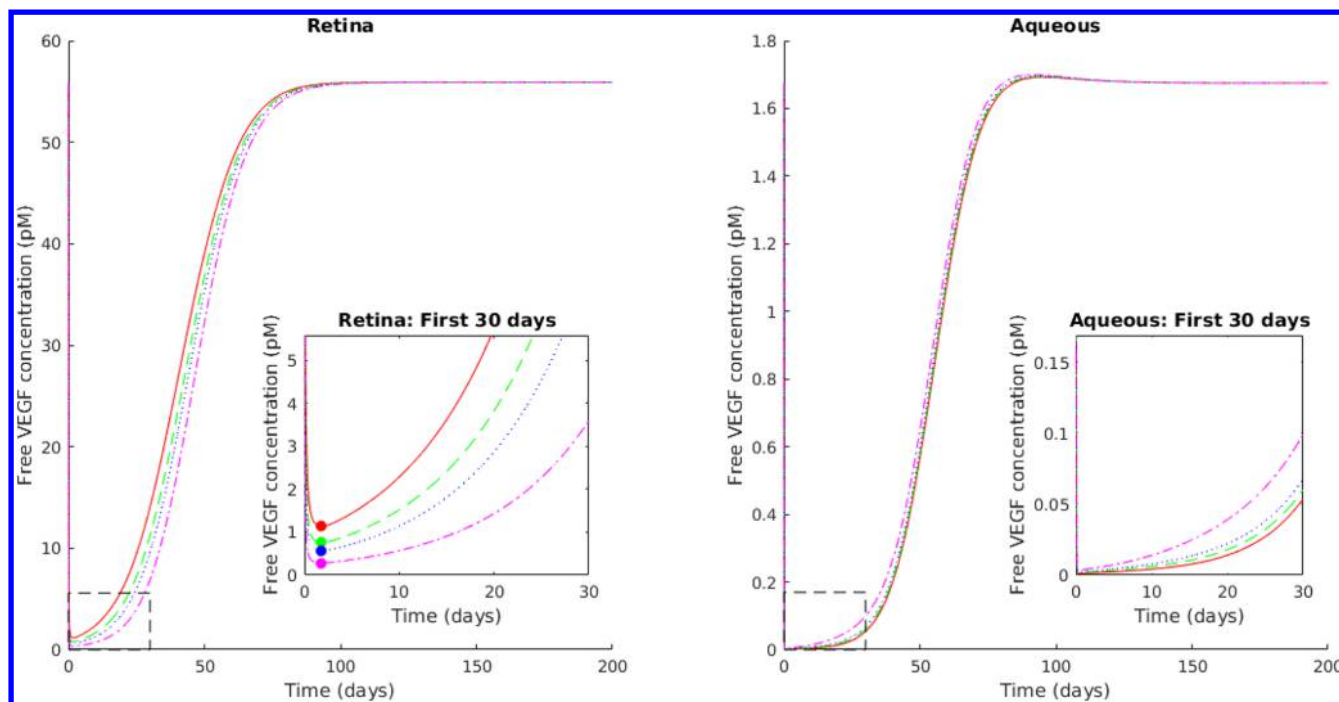


**Figure 13.** Simulated effect of increasing  $k_{on}$  and  $k_{off}$  with  $K_D$  fixed at 19 000 pM. Plots shown correspond to  $k_{off} = 0.864 \text{ day}^{-1}$  (solid red),  $k_{off} = 1.296 \text{ day}^{-1}$  (dashed green),  $k_{off} = 1.728 \text{ day}^{-1}$  (dotted blue), and  $k_{off} = 3.456 \text{ day}^{-1}$  (dot-dash magenta).

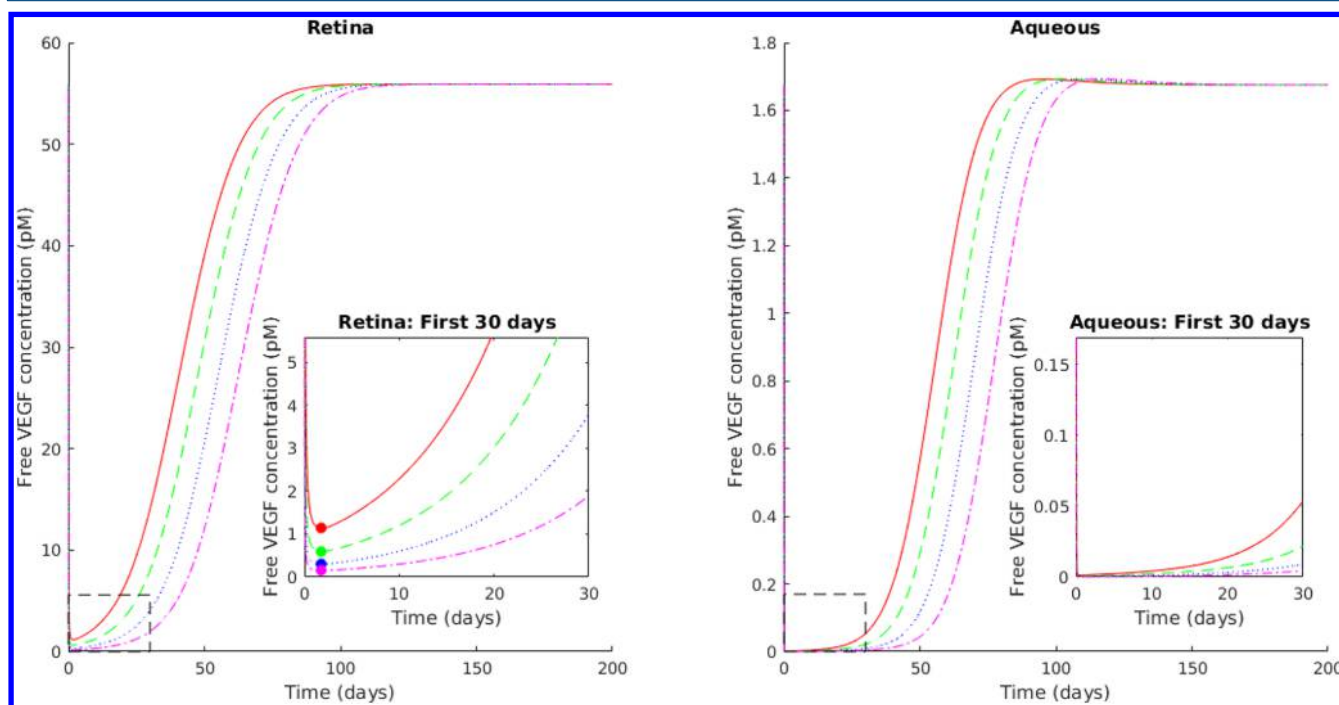


**Figure 14.** Simulated effect of increasing  $k_{on}$  and decreasing  $K_D$  with  $k_{off}$  fixed at  $0.864 \text{ day}^{-1}$ . Plots shown correspond to  $K_D = 19\,000 \text{ pM}$  (solid red),  $K_D = 10\,000 \text{ pM}$  (dashed green),  $K_D = 5000 \text{ pM}$  (dotted blue), and  $K_D = 2500 \text{ pM}$  (dot-dash magenta).

considered any observed concentration in the aqueous “below the lower limit of quantification, LOQ (4 pg/mL, or 0.1 pM) of the Luminex xMAP assay” to indicate a clinically suppressed state. The predicted minimum free VEGF concentration in the retina averaged roughly 1 pM across the patient sample; this value is 10 times greater than the previously considered “suppressed level” of 0.1 pM used by Saunders et al.<sup>10</sup> All simulations indicated that this minimum was achieved at early time (roughly 2 days) and was subsequently followed by an

exponential increase in free VEGF at a rate equal to that of the removal of ranibizumab from the system (as shown by eq S.85 in the Supporting Information). A potential hypothesis for the biologically relevant free VEGF suppression level may be derived by considering the dissociation constant between VEGF and VEGF receptor molecules. Levels of free retinal VEGF below this dissociation constant would correspond to a majority of VEGF receptors left unbound and, hence, may represent a biologically relevant threshold. Literature on  $K_D$  for

VEGF-R binding shows a wide variation from nM values<sup>28–30</sup> to pM values.<sup>31</sup> More data are needed to clarify this key parameter in order to assess the biological relevance of the retinal suppression curves.

Using the three-compartment model, we have explored the effect of dose on the VEGF profiles in the aqueous humor and retina and compared these predictions to available clinical data. As can be seen in Figure 11, increasing the dose of an anti-VEGF molecule is predicted to prolong the duration of VEGF suppression in both compartments and also increase the depth of VEGF suppression in the retina. For each doubling of the dose, the model predicts that the free VEGF profiles will shift to the right by approximately one ocular half-life of the anti-VEGF molecule and the minimum VEGF concentration in the retina will decrease by 50% (Figure 11). For patients with higher values of  $p_{RPE}$  (Figure 10a), whose retinal VEGF suppression is attenuated, a higher dose may improve the clinical response (Figure 10c). In this regard two clinical studies—HARBOR and SAVE—have investigated the effects of 2 mg vs 0.5 mg doses of ranibizumab in monthly and/or PRN (as needed) regimens in patients with wet AMD. At the 24-month end point of the HARBOR study (Ho et al., 2014<sup>32</sup>), the mean number of injections administered to patients who completed the study was 11.9 in the 2 mg PRN group vs 14.2 in the 0.5 mg PRN group. The corresponding average interval between injections was 12.5 weeks in the 2 mg PRN group vs 9.9 weeks in the 0.5 mg PRN group, a difference of 2.6 weeks. The two PRN treatment groups had comparable results on the visual acuity end points (change from baseline in BCVA) at the 12- and 24-month evaluations, approximately +8 letters. According to the model, a 4-fold increase in dose should increase the duration of VEGF suppression after each injection by approximately two half-lives, which for ranibizumab is about 16 days (2.3 weeks). This prediction is consistent with the longer injection interval observed in the HARBOR study for the 2 mg PRN group. In the SAVE study (Brown et al., 2013<sup>33</sup>), so-called “recalcitrant patients” with persistent leakage on standard monthly doses of ranibizumab (0.5 mg) or bevacizumab (1.25 mg) were given three consecutive monthly doses of 2 mg of ranibizumab and evaluated one month after each dose. At these times points the average change in BCVA from the baseline level achieved on standard dosing ranged between +3.3 and +3.9 letters. This finding would be consistent with a longer or deeper retinal VEGF suppression at the 2 mg dose, as expected from Figure 10c. As suggested by Brown et al., such “recalcitrant patients” may either have a shorter ocular half-life of ranibizumab or require a greater degree of VEGF blockade.<sup>33</sup> In terms of the three-compartment model, such patients could conceivably have a higher RPE permeability that would shorten their ocular half-life and result in a lower degree of retinal VEGF suppression (Figure 10a).

In our previous and current analyses of the experimental aqueous humor VEGF profiles, we assumed the  $k_{off}$  value for ranibizumab to be 0.864 day<sup>-1</sup> based on Yang's *in vitro* estimate.<sup>14</sup> Here we discuss effects of varying the binding parameters  $k_{off}$ ,  $k_{on}$ , and  $K_D$  on the aqueous and retinal VEGF profiles. As can be seen in Figure 12, decreasing  $k_{off}$  with a fixed  $k_{on}$ , i.e., lowering  $K_D$ , shifts the aqueous VEGF profiles to the right (as in the two-compartment model) but has a much weaker effect on the retinal VEGF profile. Increasing  $k_{off}$  and  $k_{on}$  in parallel, i.e., keeping  $K_D$  constant, has no effect on the aqueous VEGF profile (as in the two-compartment model) and only a weak influence on the retinal VEGF profile (Figure 12).

Lastly, increasing  $k_{on}$  with a fixed  $k_{off}$ , i.e., also decreasing  $K_D$ , shifts both the aqueous and retinal VEGF profiles to the right and also deepens the retinal profile (Figure 13). The latter result is completely analogous to the effect of increasing dose on the VEGF profiles (Figure 11). The parallel effects of increasing  $k_{on}$  and dose are explained theoretically in Section S6 of the Supporting Information, where it is shown explicitly that the minimum VEGF concentration attained in the retina will be inversely proportional to both the dose and  $k_{on}$ . These simulations further illustrate conditions where changes in the aqueous humor VEGF profile may not be reflected in the retinal VEGF profile and vice versa.

In summary, we have extended our previous two-compartment ocular PK/PD model of the vitreous and aqueous humors to a three-compartment model that includes the retina. Using this new model, we have re-analyzed Sanders's aqueous humor VEGF profiles in wet AMD patients to re-estimate the  $K_D$  value for ranibizumab and characterize the variability in the aqueous suppression profile and the simulated retinal suppression profiles. We have explored the sensitivity of the model to the assumed value of the RPE permeability value. For the reference value estimated from PK data in rabbit, we observe a 50% shorter duration of VEGF suppression in the retina than in the aqueous humor. We believe this finding could explain the shorter duration of disease activity in the patients characterized by Fauser et al. as having a high anti-VEGF demand. However, the RPE permeability could conceivably be higher or lower than this reference value, depending on the extent of penetration of the RPE by neovascularization and/or the presence of large drusen or other pathology. In the case of low RPE permeability, the VEGF profiles in the retina and aqueous humor show a comparable duration of suppression. At very high RPE permeability, the duration of retinal suppression is much shorter and less deep. The latter case may reflect the “recalcitrant AMD patients” described by Brown. We believe that our three-compartment model provides new theoretical insights into ocular PK/PD that may guide the future development of new dosing regimens and new molecules.

## ■ ASSOCIATED CONTENT

### 📄 Supporting Information

The Supporting Information is available free of charge on the ACS Publications website at DOI: 10.1021/acs.molpharmaceut.8b00280.

Estimation of hydrodynamic radii of R, V, VR, and RVR species; vitreous–aqueous clearance parameters; initial conditions; individual patient plots; relationship between  $t_{1/2}^{(r)}$  and  $K_D$ ; and asymptotic analysis (PDF)

## ■ AUTHOR INFORMATION

### Corresponding Authors

\*E-mail: laurence.hutton-smith@pmb.ox.ac.uk.

\*E-mail: norman.mazer@roche.com.

### ORCID

Antonello Caruso: 0000-0001-5832-3636

Norman A. Mazer: 0000-0003-3759-0115

### Author Contributions

N.A.M., E.A.G., L.A.H.-S., P.K.M., A.C., and H.M.B. designed the study. L.A.H.-S. carried out the analysis. N.A.M., E.A.G., P.K.M., A.C., and H.M.B. provided input to the analysis and collaborated on the discussion.

## Notes

The authors declare the following competing financial interest(s): N. Mazer and A. Caruso are employees and shareholders of F. Hoffmann-La Roche.

## ACKNOWLEDGMENTS

This work was supported by funding from the Engineering and Physical Sciences Research Council (EPSRC) and the Medical Research Council (MRC) [grant number EP/L016044/1]. Additional funding was provided by Roche Pharma Research and Early Development. The authors thank Dietmar Schwab for careful reading of this manuscript and helpful suggestions.

## REFERENCES

- (1) Wong, W. L.; Su, X.; Li, X.; Cheung, C. M. G.; Klein, R.; Cheng, C.-Y.; Wong, T. Y. Global prevalence of age-related macular degeneration and disease burden projection for 2020 and 2040: A systematic review and meta-analysis. *Lancet Global Health* **2014**, *2* (2), e106–e116.
- (2) Ambati, J.; Fowler, B. J. Mechanisms of age-related macular degeneration. *Neuron* **2012**, *75* (1), 26–39.
- (3) Ferrara, N. Vascular endothelial growth factor and age-related macular degeneration: from basic science to therapy. *Nat. Med.* **2010**, *16* (10), 1107–1111.
- (4) Penn, J. S.; Madan, A.; Caldwell, R. B.; Bartoli, M.; Caldwell, R. W.; Hartnett, M. E. Vascular endothelial growth factor in eye disease. *Prog. Retinal Eye Res.* **2008**, *27* (4), 331–371.
- (5) van Lookeren Campagne, M.; LeCouter, J.; Yaspan, B. L.; Ye, W. Mechanisms of age-related macular degeneration and therapeutic opportunities. *Journal of pathology* **2014**, *232* (2), 151–164.
- (6) Muether, P. S.; Hermann, M. M.; Dröge, K.; Kirchhof, B.; Fauser, S. Long-term stability of vascular endothelial growth factor suppression time under ranibizumab treatment in age-related macular degeneration. *Am. J. Ophthalmol.* **2013**, *156* (5), 989–993.
- (7) Fauser, S.; Muether, P. S. Clinical correlation to differences in ranibizumab and aflibercept vascular endothelial growth factor suppression times. *Br. J. Ophthalmol.* **2016**, *100* (11), 1494–1498.
- (8) Hutton-Smith, L. A.; Gaffney, E. A.; Byrne, H. M.; Maini, P. K.; Gadkar, K.; Mazer, N. A. Ocular Pharmacokinetics of Therapeutic Antibodies Given by Intravitreal Injection: Estimation of Retinal Permeabilities Using a 3 Compartment Semi-Mechanistic Model. *Mol. Pharmaceutics* **2017**, *14*, 2690–2696.
- (9) Hutton-Smith, L. A.; Gaffney, E. A.; Byrne, H. M.; Maini, P. K.; Schwab, D.; Mazer, N. A. A mechanistic model of the intravitreal pharmacokinetics of large molecules and the pharmacodynamic suppression of ocular VEGF levels by ranibizumab in patients with neovascular age-related macular degeneration. *Mol. Pharmaceutics* **2016**, *13* (9), 2941–2950.
- (10) Saunders, D. J.; Muether, P. S.; Fauser, S. A model of the ocular pharmacokinetics involved in the therapy of neovascular age-related macular degeneration with ranibizumab. *Br. J. Ophthalmol.* **2015**, *99* (11), 1554–1559.
- (11) Ferrara, N.; Damico, L.; Shams, N.; Lowman, H.; Kim, R. Development of ranibizumab, an anti-vascular endothelial growth factor antigen binding fragment, as therapy for neovascular age-related macular degeneration. *Retina* **2006**, *26* (8), 859–870.
- (12) Gadkar, K.; Pastuskovas, C. V.; Le Couter, J. E.; Elliott, J. M.; Zhang, J.; Lee, C. V.; Sanowar, S.; Fuh, G.; Kim, H. S.; Lombana, T. N.; Spiess, C.; Nakamura, M.; Hass, P.; Shatz, W.; Meng, Y. G.; Scheer, J. M. Design and pharmacokinetic characterization of novel antibody formats for ocular therapeutics. *Invest. Ophthalmol. Visual Sci.* **2015**, *56* (9), 5390–5400.
- (13) Halfter, W.; Dong, S.; Dong, a; Eller, a W; Nischt, R. Origin and turnover of ECM proteins from the inner limiting membrane and vitreous body. *Eye (London, U. K.)* **2008**, *22* (10), 1207–1213.
- (14) Yang, J.; Wang, X.; Fuh, G.; Yu, L.; Wakshull, E.; Khosraviani, M.; Day, E. S.; Liu, J.; Shire, S. J.; Ferrara, N.; Yadav, S. Comparison of

binding characteristics and in vitro activities of three inhibitors of vascular endothelial growth factor A. *Mol. Pharmaceutics* **2014**, *11*, 3421–3430.

- (15) Tasman, W.; Jaeger, E. A. *Duane's Ophthalmology 2013*; Lippincott Williams & Wilkins: Philadelphia, 2013.

- (16) Krohne, T. U.; Eter, N.; Holz, F. G.; Meyer, C. H. Intraocular pharmacokinetics of bevacizumab after a single intravitreal injection in humans. *Am. J. Ophthalmol.* **2008**, *146* (4), 508–512.

- (17) Zhu, Q.; Ziemssen, F.; Henke-fahle, S.; Tatar, O.; Szurman, P.; Aisenbrey, S.; Schneiderhan-marra, N.; Xu, X.; Grisanti, S. Vitreous levels of bevacizumab and vascular endothelial growth factor-A in patients with choroidal neovascularization. *Ophthalmology* **2008**, *115*, 1750–1755.

- (18) Fontana, S. T.; Brubaker, R. F. Volume and depth of the anterior chamber in the normal aging human eye. *Arch. Ophthalmol.* **1980**, *98*, 1803–1808.

- (19) Toris, C. B.; Yablonski, M. E.; Wang, Y.-L.; Camras, C. B. Aqueous humor dynamics in the aging human eye. *Am. J. Ophthalmol.* **1999**, *127* (4), 407–412.

- (20) Missel, P. J. Simulating intravitreal injections in anatomically accurate models for rabbit, monkey, and human eyes. *Pharm. Res.* **2012**, *29* (12), 3251–3272.

- (21) *MATLAB user guide R2015b: Global Optimization Toolbox*; The MathWorks Inc.: Natick, MA, 2015.

- (22) Bolton, S.; Bon, C. *Pharmaceutical Statistics: Practical and Clinical Applications*, 4th ed.; Marcel Dekker: New York, 2004.

- (23) Heiduschka, P.; Fietz, H.; Hofmeister, S.; Schultheiss, S.; Mack, A. F.; Peters, S.; Ziemssen, F.; Niggemann, B.; Julien, S.; Bartz-Schmidt, K. U.; Schraermeyer, U. Penetration of bevacizumab through the retina after intravitreal injection in the monkey. *Invest. Ophthalmol. Visual Sci.* **2007**, *48* (6), 2814–2823.

- (24) Pitkänen, L.; Ranta, V.-P.; Moilanen, H.; Urtti, A. Permeability of retinal pigment epithelium: Effects of permeant molecular weight and lipophilicity. *Invest. Ophthalmol. Visual Sci.* **2005**, *46* (2), 641–646.

- (25) Moja, L.; Lucenteforte, E.; Kwag, K. H.; Bertele, V.; Campomori, A.; Chakravarthy, U.; D'Amico, R.; Dickersin, K.; Kodjikian, L.; Lindsley, K.; Loke, Y.; Maguire, M.; Martin, D. F.; Mugelli, A.; Mühlbauer, B.; Püntmann, I.; Reeves, B.; Rogers, C.; Schmucker, C.; Subramanian, M. L.; Virgili, G. Systemic safety of bevacizumab versus ranibizumab for neovascular age-related macular degeneration. *Cochrane Database of Systemic Reviews* **2014**, *7*, CD011230.

- (26) Tilton, R. D. The Conformation of the Poly(ethylene glycol) Chain in Mono-PEGylated Lysozyme and Mono-PEGylated Human Growth Hormone. *Bioconjugate Chem.* **2011**, *22*, 2317–2323.

- (27) Muether, P. S.; Hermann, M. M.; Viebahn, U.; Kirchhof, B.; Fauser, S. Vascular endothelial growth factor in patients with exudative age-related macular degeneration treated with ranibizumab. *Ophthalmology* **2012**, *119* (10), 2082–2086.

- (28) Waltenberger, J.; Claesson-Welsh, L.; Siegbahn, A.; Shibuya, M.; Heldin, C.-H. Different Signal-Transduction Properties of Kdr and Flt1, 2 Receptors for Vascular Endothelial Growth-Factor. *J. Biol. Chem.* **1994**, *269* (43), 26988–26995.

- (29) Leppänen, V.-M.; Prota, A. E.; Jeltsch, M.; Anisimov, A.; Kalkkinen, N.; Strandin, T.; Lankinen, H.; Goldman, A.; Ballmer-Hofer, K.; Alitalo, K. Structural determinants of growth factor binding and specificity by VEGF receptor 2. *Proc. Natl. Acad. Sci. U. S. A.* **2010**, *107* (6), 2425–2430.

- (30) Quinn, T. P.; Peters, K. G.; De Vries, C.; Ferrara, N.; Williams, L. T. Fetal liver kinase 1 is a receptor for vascular endothelial growth factor and is selectively expressed in vascular endothelium. *Proc. Natl. Acad. Sci. U. S. A.* **1993**, *90* (16), 7533–7.

- (31) Papadopoulos, N.; Martin, J.; Ruan, Q.; Rafique, A.; Rosconi, M. P.; Shi, E.; Pyles, E. A.; Yancopoulos, G. D.; Stahl, N.; Wiegand, S. J. Binding and neutralization of vascular endothelial growth factor (VEGF) and related ligands by VEGF Trap, ranibizumab and bevacizumab. *Angiogenesis* **2012**, *15* (2), 171–185.

- (32) Ho, A. C.; Busbee, B. G.; Regillo, C. D.; Wieland, M. R.; Van Everen, S. A.; Li, Z.; Rubio, R. G.; Lai, P. Twenty-four-month efficacy

and safety of 0.5 mg or 2.0 mg ranibizumab in patients with subfoveal neovascular age-related macular degeneration. *Ophthalmology* **2014**, *121* (11), 2181–2192.

(33) Brown, D. M.; Chen, E.; Mariani, A.; Major, J. C. Super-dose anti-VEGF (SAVE) trial: 2.0 mg Intravitreal ranibizumab for recalcitrant neovascular macular degeneration-primary end point. *Ophthalmology* **2013**, *120* (2), 349–354.